The Cryogenic AntiCoincidence detector for ATHENA X-IFU: a program overview

Macculi, C., Argan, A., D'Andrea, M., Lotti, S., Laurenza, M., et al.

C. Macculi, A. Argan, M. D'Andrea, S. Lotti, M. Laurenza, L. Piro, M. Biasotti, D. Corsini, F. Gatti, G. Torrioli, M. Fiorini, S. Molendi, M. Uslenghi, T. Mineo, A. Bulgarelli, V. Fioretti, E. Cavazzuti, "The Cryogenic AntiCoincidence detector for ATHENA X-IFU: a program overview," Proc. SPIE 9905, Space Telescopes and Instrumentation 2016: Ultraviolet to Gamma Ray, 99052K (18 July 2016); doi: 10.1117/12.2231298

SPIE.

Event: SPIE Astronomical Telescopes + Instrumentation, 2016, Edinburgh, United Kingdom

The Cryogenic AntiCoincidence Detector for ATHENA X-IFU: a program overview

C. Macculi*[a], A. Argan[a] , M. D'Andrea[a], S. Lotti[a], M. Laurenza [a], L. Piro[a] , M. Biasotti[b], D. Corsini[b], F. Gatti[b], G. Torrioli[c], M. Fiorini[d], S. Molendi[d], M. Uslenghi[d], T. Mineo[e], A. Bulgarelli[f], V. Fioretti[f], E. Cavazzuti[g]

[a] INAF/IAPS Roma, Via del Fosso del Cavaliere 100, 00133 Roma, Italia
[b] Dipartimento di Fisica, Università di Genova, Via Dodecaneso 33, 16146 Genova, Italia
[c] Istituto di Fotonica e Nanotecnologie - CNR, Via Cineto Romano 42, 00156 Roma, Italia
[d] INAF/IASF Milano, Via E. Bassini 15, 20133 Milano, Italia
[e] INAF-IASF Palermo, Via Ugo La Malfa 153, 90146 Palermo, Italia
[f] INAF-IASF Bologna, Via P. Gobetti 101, 40129 Bologna, Italia
[g] ASI, Via del Politecnico snc, 00133 Roma, Italia

ABSTRACT

The ATHENA observatory is the second large-class ESA mission, in the context of the Cosmic Vision 2015 - 2025, scheduled to be launched on 2028 at L2 orbit. One of the two on-board instruments is the X-IFU (X-ray Integral Field Unit): it is a TES-based kilo-pixels order array able to perform simultaneous high-grade energy spectroscopy (2.5 eV at 6 keV) and imaging over the 5 arcmin FoV. The X-IFU sensitivity is degraded by the particles background which is induced by primary protons of both solar and Cosmic Rays origin, and secondary electrons. The studies performed by Geant4 simulations depict a scenario where it is mandatory the use of reduction techniques that combine an active anticoincidence detector and a passive electron shielding to reduce the background expected in L2 orbit down to the goal level of 0.005 cts/cm^2/s/keV, so enabling the characterization of faint or diffuse sources (e.g. WHIM or Galaxy cluster outskirts). From the detector point of view this is possible by adopting a Cryogenic AntiCoincidence (CryoAC) placed within a proper optimized environment surrounding the X-IFU TES array. It is a 4-pixels detector made of wide area Silicon absorbers sensed by Ir TESes, and put at a distance < 1 mm below the TES-array. On October 2015 the X-IFU Phase A program has been kicked-off, and about the CryoAC is at present foreseen on early 2017 the delivery of the DM1 (Demonstration Model 1) to the FPA development team for integration, which is made of 1 pixel "bridges-suspended" that will address the final design of the CryoAC. Both the background studies and the detector development work is on-going to provide confident results about the expected residual background at the TES-array level, and the single pixel design to produce a detector for testing activity on 2016/2017. Here we will provide an overview of the CryoAC program, discussing some details about the background assessment having impact on the CryoAC design, the last single pixel characterization, the structural issues, followed by some programmatic aspects.

Keywords: Cryogenic detectors, Anticoincidence, Particle background, ATHENA, TES, Geant4.

1. INTRODUCTION

The ATHENA (Advanced Telescope for High ENergy Astrophysics)[1] satellite will have on board two instruments, the X-IFU[2] and the WFI[3] aimed at providing exhaustive answers to the following astrophysical questions:

* claudio.macculi@iaps.inaf.it; phone +39 0649934658; fax +39 06 45488188; www.iaps.inaf.it

Space Telescopes and Instrumentation 2016: Ultraviolet to Gamma Ray, edited by Jan-Willem A. den Herder, Tadayuki Takahashi, Marshall Bautz, Proc. of SPIE Vol. 9905, 99052K
 · doi: 10.1117/12.2231298

- How does ordinary matter assemble into the large-scale structures we see today?
- How do black holes grow and shape the Universe?

The two instruments are complementary each other: the first one will provide detailed image over FoV of 5 arcmin featured by very high spectral energy resolution (2.5eV@6keV) generating for the first time the so-called "Integral field spectroscopy", whereas the second will provide image over a wider FoV (40'x40') but with lower energy resolution (< 150eV@6keV).
One of the X-IFU scientific aim, the reference instrument for this work, it is to provide high spectral energy resolution map of faint or diffuse sources. Hence a very low particle residual background (bkg) around its TES-array detector is necessary. Particle reduction techniques have to be adopted to reduce the bkg at the L2 orbit by a factor 10^2 down to the goal of 0.005 cts/cm^2/s/kev [4]. Such techniques are constituted by an active Cryogenic AntiConcidence detector (CryoAC), and a passive electron shielding surrounding the TES-array.

Is this paper the following arguments will be discussed: bkg assessment and secondaries reduction by a passive shielding through Geant4 simulations, and direct impact on the CryoAC design (energy range, assessment on deadtime); the CryoAC instrument: h/w development (detector + electronics); CryoAC characterization: last design aspects (Silicon beams mask), and last single pixel measurement (AC-S7) and related data analysis by the PCA method; Structural issues: some aspects about modal analysis, and vibration issues; and at last Programmatic aspects: some info about the schedule for the next activities.

2. BKG ASSESSMENT AT THE FPA AND ITS IMPACT ON THE CRYOAC DESIGN

2.1 L2 environment assessment and Geant4 simulation.

No X-ray instruments have ever been inserted into a L2 orbit, and few satellites (e.g., Planck and Herschel having on board the SREM monitor[5], or transiting close/through L2 by Geotail[6] or Wind[7]) have collected useful data to properly characterize the L2 environment as required for a x-ray mission. The contribution to the bkg is mainly divided in two categories: the so called "Soft Proton/ions" (E < few hundred's keV) components whose origin is from the Sun and L2 magnetotail, that can be collimated by grazing incidence by X-ray optics towards the focal plane assembly (FPA), and the GCRs (hundred's MeV to GeV) that crossing the satellites over 4π sr arrive at the focal plane, producing also secondaries. Both components deposit energy within the main detector energy range. In order to get the expected particle bkg surrounding the main detector, simulations by Monte Carlo method using the Geant4 toolkit have to be performed: such a primary flux is to interact with the mass model of the payload to produce the expected bkg estimate.

In order to have the best guess on the expected environment in L2 orbit, all the data from several satellites, not only x-ray payload, not only orbiting in L2, but also in L1 orbit, LEO, etc…, are collected and analyzed, than "transferred" by a properly scaling to L2 when possible. This is the main goal of the scientific part of the AREMBES activity, just started, performed by an ESA contract. It encompasses the bkg X-IFU workpackage activity since it improves and extends the L2 characterization tasks, the verification and validation tasks of Geant4 physics routines in order to increase the confidence level of the produced results, all of this thanks also to the involvement of the WFI team.

The low energy particle environment in L2 is expected to be quite complex since the magnetospheric structure is not homogeneous nor stationary being determined by the state of the solar wind[8], but a magnetic diverter is foreseen on the ATHENA satellite to efficiently deflect this contribution far from the FPA. Instead, since the CGR have high energies, it is expected that this component is not so strongly interacting with the L2 magnetospheric environment, so the usual stationary flux measured in different orbit can be used to infer the expected particle bkg around the main detector by means of the Geant4 simulation. At present, the provided residual bkg takes into account only the CGR component.

We report in Fig. 1 the new implementation of the FPA that has been simulated by Geant4 [9]. One of the most interesting item is the electron liner (in gray, Fig. 1 - Right) necessary to reduce the electron contribution towards the TES array: it reduces secondary e^- produced by primaries crossing the Niobium shield (in blue), generating a lower number of secondary electrons. Fig. 2 – Left, shows a breakdown of the various particles impacting the TES-array. Together with photons, the electrons backscattered onto the top surface of the TES-array are the main contribution to the residual background since they are not detected by the CryoAC. By means of a careful design of the electron liner, such

components can be further reduced starting from the baseline configuration of only Kapton, through an adoption of a bilayer Si3N4-Kapton or Bi-Kapton, as reported in Fig. 2 – Right, or substituting the lower section of the liner with an higher density material [9]. The residual bkg is then reduced down to about 0.008 cts/cm^2/s/keV close to the scientific requirement (less than a factor 2).

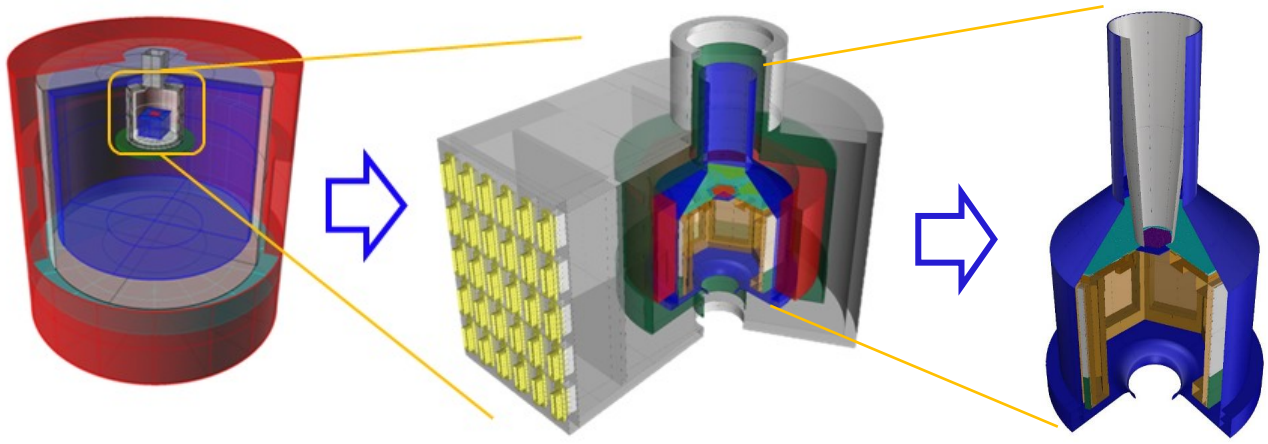

Figure 1. Left - Preliminary cryostat mass model (credits SRON). Centre - New FPA mass model (CAD) – Right – A detail of the 50 mK FPA. In grey it is shown the electron liner (Color figure online).

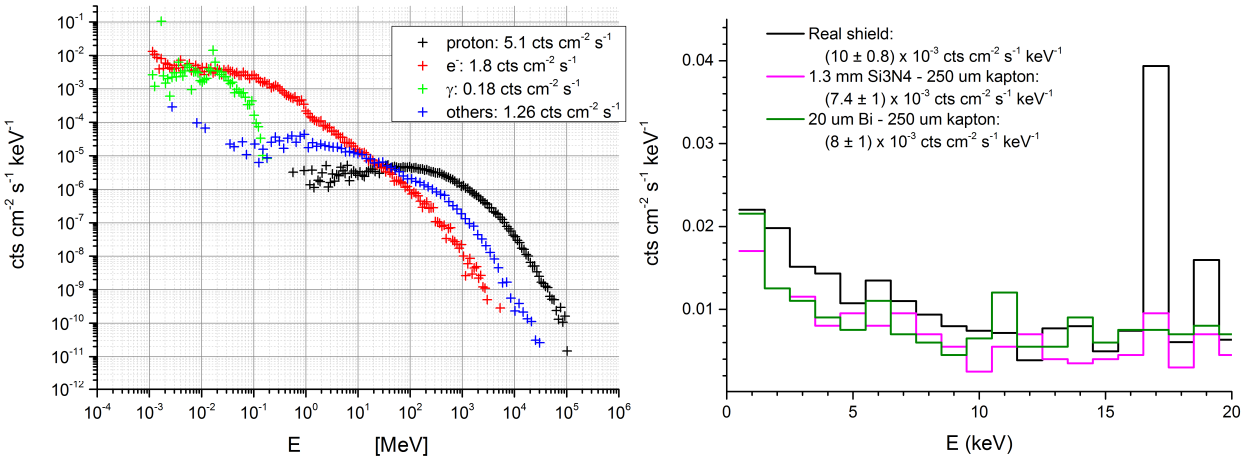

Figure 2. Left- Energy spectra of particles impacting on the TES-array. Right – Comparison of the residual particle bkg among 3 different configurations of the electron liner. The "Real shield" is the baseline: only Kapton 250 μm thick (Color figure online).

2.2 The CryoAC Requirements and Specifications

Parallel to the bkg evaluation at the TES array level, Geant4 simulation are necessary to design the CryoAC detector in order to fulfill the scientific requirement. This is not the context to provide an exhaustive discussion about the CryoAC instrument requirements that translate into detector specifications (see Tables 1 and 2), but some words can be spent about one of its most important parameters having also an impact on the TES-array functioning, its intrinsic Dead Time (DT) that could constitute part of the TES array DT: it is a discussion already in place inside the X-IFU System Team as expected along the Phase A of the program. The CryoAC main goal is to reject particle bkg, that is to increase the rejection efficiency. Since the CryoAC is sensed by a TES detector, it is necessary to identify two working regimes: inside and outside the transition (i.e., saturation).

Table 1. CryoAC Instrument Requirements.

Parameter	Value
Geometrical rejection efficiency (weighted average among primaries and secondaries).	98.5% (TBC) at 1 mm distance between the "TES sensor of the TES-array" and the "top CryoAC absorber surface".
Low Energy Threshold	20 keV (TBC)
Detector Dynamic Energy range	5 keV – 750 keV (TBC)
Data Acquistion Dynamic range	0 – 1000 keV (TBC)
Time tagging accuracy	10 μs (TBC)
Time tagging resolution	TBD μs at 3 sigma error (TBC)
Intrinsic Deadtime	2%@ < 9.15 cts/cm^2/s (TBC)
Induced Deadtime towards the TES array.	TBD

Table 2. CryoAC detector specifications (current baseline) to be updated.

Parameter	Value
Number of Pixels	4
Pixel size	1.15 cm^2
Thickness	500 μm
Distance from X-IFU	< 1 mm
Detector Dynamic Energy range	5 keV – 750 keV (TBC)
Data Acquistion Dynamic range	0 – 1000 keV (TBC)
Rise Time	< 30 μs (TBC)
Effective Fall time constant	250 μs (TBC)
Thermal time constant	< 2.5 ms
TES Material	Ir/Au (TBC)
Absorber Material	Silicon
Transition temperature	80-100 mK (TBC)
Thermal bath temperature	50-55 mK
TES normal resistance Rn	10 mΩ (TBC)
TES working point resistance	0.1-0.2 × Rn
Frequency Bandwidth	5 kHz (TBC)
Slew Rate	< 20 A/s (TBC) f1 = 1 MHz (Unity gain frequency)

Inside the transition, whose width is defined by the CryoAC maximum energy (E_{max}), the detector is able to generate impulsive response, and it responds with the ETF (Electro-Thermal Feedback) as decay constant. To flag and tag the bkg events the rise front of the developed pulse is used. The veto window to be applied in transition is a combination between the TES array and the CryoAC timings/accuracy, but from the CryoAC point of view its peaking time (TBC) could be adopted. At present it is required as CryoAC rise time τ_R = 30 μs (TBC), so a peaking time or CryoAC Veto time in transition of about 100 μs. Alternative techniques are in place to be studied in order to reduce this window.

Outside the transition, due to events depositing energy greater than E_{max}, the CryoAC is blind and by definition it charges DT meaning that the detector is inefficient (the TES cannot work): if now the CryoAC system does not apply the veto, all the events inside this window will not be rejected so increasing the bkg. Hence, the veto duration should be addressed by the CryoAC recovery time t_{rec} which is the time to be able to re-trigger again. It's the sum between the "thermal" time

constant (no ETF) corrected by the E_d deposited energy-to-E_{max} ratio, and the ETF decay time when it re-enters in the transition (τ_{ETF}):

$$t_{rec} = m_{sat} \cdot \tau_{ETF} + \tau_{th} \cdot \ln\left(\frac{E_{dep}}{E_{max}}\right) \quad (1)$$

where m_{sat} is the number of CryoAC τ_{ETF} necessary to re-trigger it again. It is possible to show that the lower is the CryoAC E_{max}, the greater is the CryoAC DT outside the transition, since it takes on board greater particle flux to be managed in saturation. By taking into account the distribution of the expected energies deposited in the CryoAC (Figure 3, Left), it is possible to assess the intrinsic total (transition + saturation) DT of the full CryoAC detector. Figure 3-Right shows that in order to have a total (in transition it is assumed 100 μs of veto time) DT = 1%, each CryoAC absorber should manage an energy bandwidth up to E_{max} = 1.2 MeV (TBC, evaluation still under study, at present 750 keV is maintained).

This approach realizes a worst but safe case scenario, and work is on-going inside the X-IFU System Team to better understand and optimize the veto window so reducing the DT.

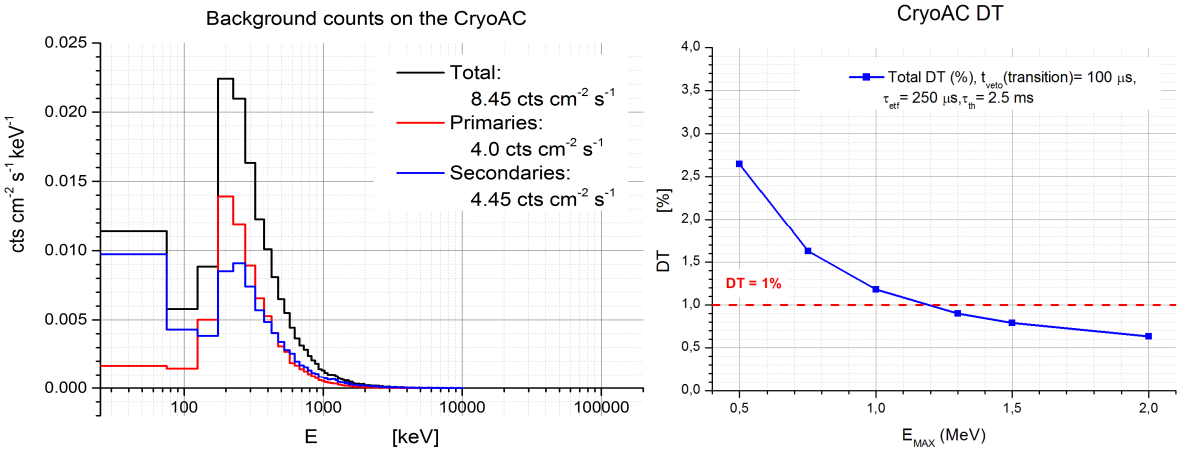

Figure 3. Left – Distribution of the expected energies deposited in the CryoAC absorber (500 um thick Silicon). Right - Expected DT vs the E_{max} for τ_{th} = 2.5 ms and veto time in transition regime (t_{veto}) equal to the pulse peaking time (Color figure online).

To conclude this section, given the above CryoAC requirements and specifications, the present design assumes that the CryoAC detector assembly is built as 4 identical trapezoidal pixels connected to a silicon rim by 3 bridges per pixel in order to realize the thermal conductance to the thermal bath, as shown in the next Fig. 4.

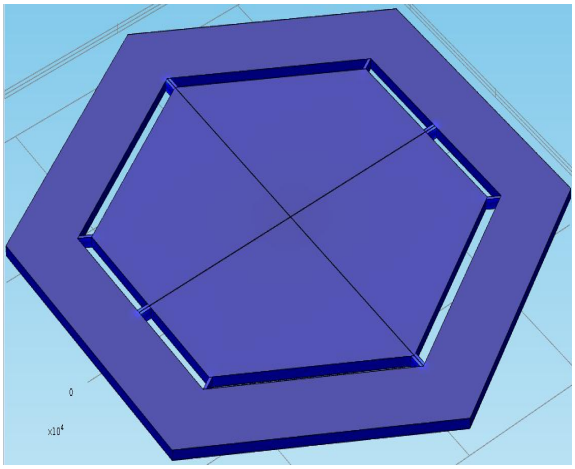

Figure 4. The CryoAC detector: 4 trapezoidal silicon pixels connected to a silicon rim by 3 bridges per pixel (Color figure online).

3. THE CRYOAC ELECTRONICS

The Figure 5 shows how it is structured the X-IFU instrument: it is shown that the data from the TES-array and the CryoAC independently each other arrive at the ICU (Instrument Control Unit), then to the spacecraft. More details can be found in Ref. 10.

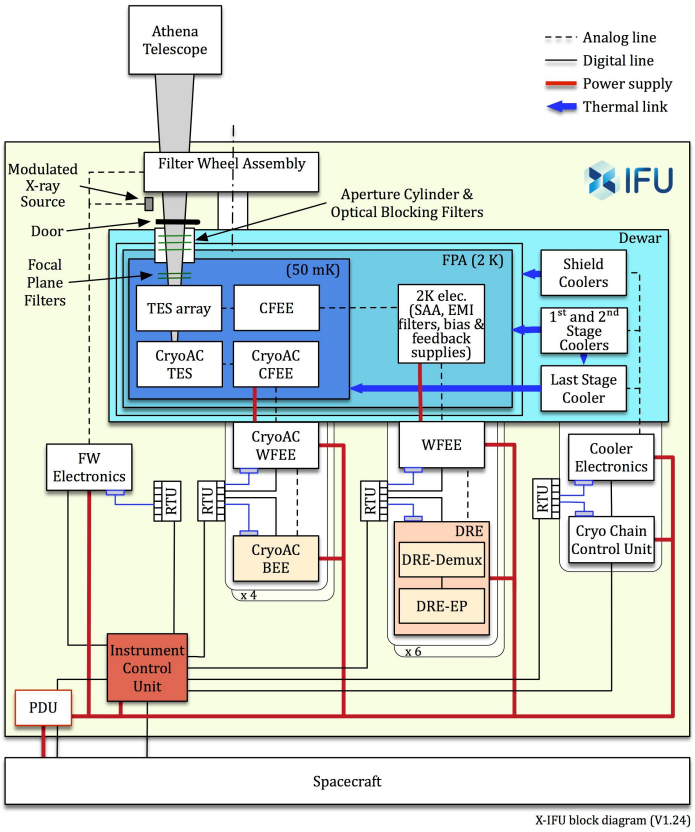

Figure 5. The X-IFU instrument block diagram (Credits IRAP) (Color figure online).

The schematic diagram concerning the CryoAC electronics implementation is shown in Figure 6. It is divided in 3 items: CFEE (Cold Front End), WFEE (Warm Front End) and WBEE (Warm Back End) Electronics.

The present baseline assumes that the CryoAC detector assembly is built as 4 identical pixels. Each of the four detectors is DC-voltage biased and readout by a dedicated SQuID. All the bias/signals in/out the FPA will be RF filtered by a dedicated cryogenic filter board at 2K. There is no multiplexing of the four pixels, and the SQuIDs are included in a standard analog FLL circuit with 1.0 MHz (TBC) bandwidth. The SQuIDs and the RF filters constitute the CFEE.

The Warm Front End electronics, powered by the PDU (Power Distribution Unit), has internal DC-DC converter to provide very clean supply. It includes the FLL circuits and the SQuIDs and TESs biasing circuitry, all in the warm (i.e. no cryo-LNA to be developed). This electronics has to be placed on board the cryostat or as close as possible to it to both reduce at the maximum level the EMI and to permit an high slew rate level of the SQuID system being limited to the wirings delay.

The Warm Back End electronics, powered by the PDU, includes the pulse detection system, the veto signals generator (VETO LOGIC) and a simple control logic. This electronics will be implemented as a dedicated unit. About the area/mass/power allocation, the FLL circuitry is deemed not critical in terms of noise and bandwidth taking in account the recently available space-qualified analog components. Also the Back End circuitry should be not critical as it is foreseen to implement it around a FPGA to include all the main digital functions.

The digital communication between the CryoAC WFEE and WBEE, and among these two units with the ICU will be realised by the RTU (Remote Terminal Unit).

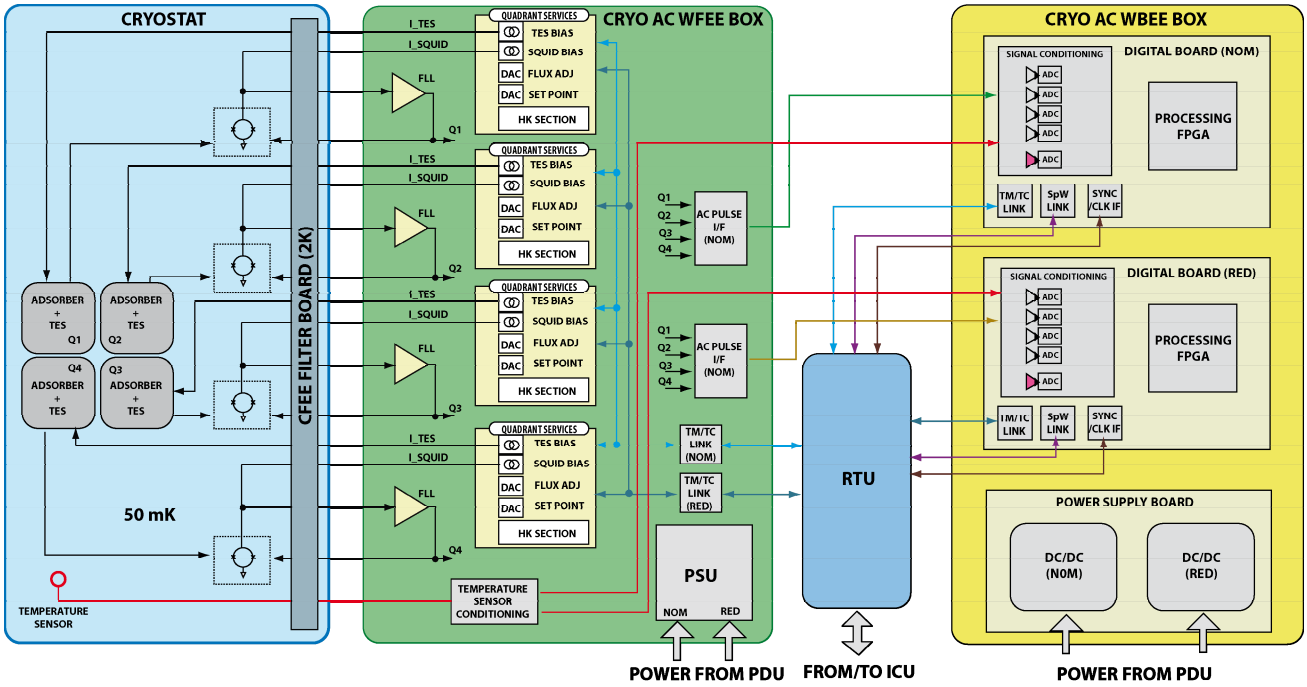

Figure 6. CryoAC electronics block diagram (Color figure online).

4. CRYOAC DEVELOPMENT AND CHARACTERIZATION

Due to the complexity of the ATHENA satellite and instruments, ESA has foreseen a milestone before the adoption where the instruments teams have to show to have reached TRL5/6. This is obviously applied to the X-IFU instrument,

and to the related critical technology such as the CryoAC and the TES array. Hence, both the instruments development is running on parallel paths that will cross at the integration epoch.

4.1 The Demonstration Model.

The first step is the production and test of the so-called DM pixel (Demonstration Model) which represents a prototype solving the critical aspects, that for the CryoAC mainly translates in developing a detector made of silicon "suspended" absorber in order to have a well reproducible thermal conductance due to its wide area, and operating it at 50 mK thermal bath temperature. The path towards the final realization of the CryoAC DM (Figure 7, Left) envisages the development and test of Silicon bridges prototypes (Figure 7, Right). Though the DM aim is to increase the detector "maturity" and it has not to be fully representative of the flight model, it will be developed filling and matching as much as possible the requirements and specifications shown in Tables 1-2.

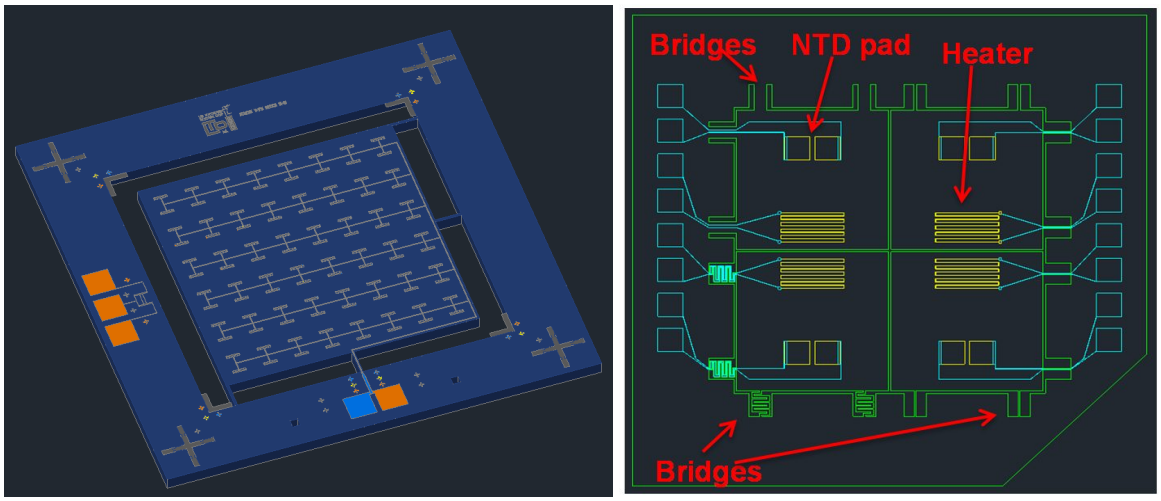

Figure 7. Left – The CryoAC DM. Right - Test structure mask: 4 different configuration of the Silicon bridge (Color figure online)

The CryoAC DM is a single pixel "bridge-suspended" detector constituted by 96 rectangular TESs laying on the Silicon chip, carved out from a 16.8x16.8 squared mm double side polished silicon wafer and suspended by 4 bridges, 100 μm wide and 1000 μm long[13]. The TESs configuration and distribution on the silicon active area (i.e., the absorber) is driven by two requirements:

- Minimize the Ir:Au volume, being the TES the leading term in the specific heat of the CryoAC
- Make uniform as much as possible the response to the A-thermal component of the primary signal generated by energy deposition due to energetic particle.

The development is ongoing.

4.2 The last single pixel measurement (AC-S7) prototype.

Before to develop the DM it's important to better understand the physics ruling the detector. In order to efficiently collect the athermal phonons[11, 12], the AC-S7 prototype has been developed and characterized. It is a 1 cm squared area pixel having on board 65 TES connected each other in parallel configuration.

Here we report some results of the activity. The pulses have been readout by both a J3-model VTT and Magnicon C6X216FB SQuIDs. More details about the recent activity can be found in Ref. 13. The main properties of the detector are shown in Table 3.

Table 3. AC-S7 main properties.

AC-S7 MAIN PARAMETERS	
Parameter	Value
Absorber Silicon Area	10 x 10 mm^2
Absorber Silicon Thickness	380 µm
TES (x65) Iridium Area	100 x 100 μm^2
TES (x65) Iridium Thickness	~ 200 nm
T_C	~ 125 mK
ΔT_C	~ 2 mK
R_N	~ 1.5 mΩ
α_{max}	~ 100

The next Fig. 8 shows a picture of the detector and some results.

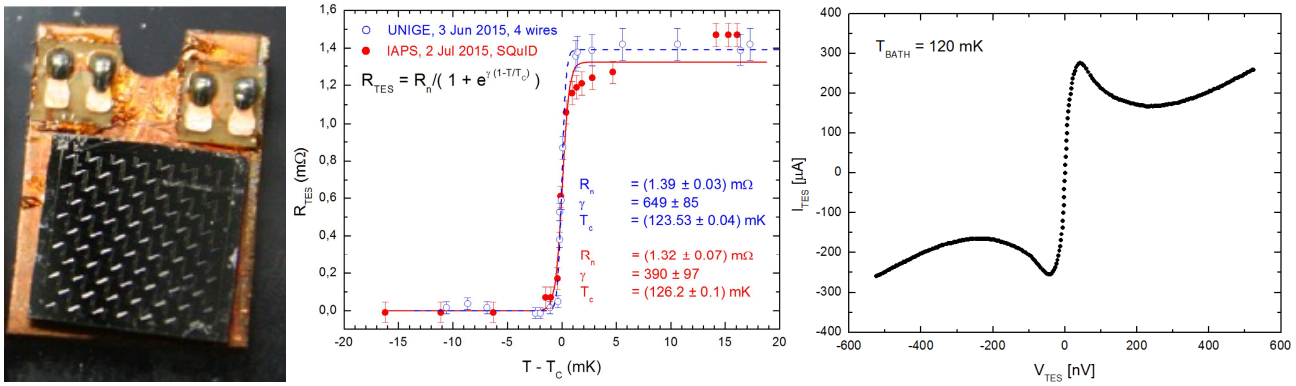

Figure 8. Left – The AC-S7 prototype. Center – Comparison between the two transition curves measured at Genova and Roma labs. Right - An example of the I-V curve (Color figure online).

The reproducibility of the R-T measurement performed in different labs setup by different techniques (SQuID and 4-wires), and the shape of the I-V curve demonstrate that the Genova laboratory has entered the right path about the manufacturing processes of these large area samples and high TES number deposition: take into account that 65 TES are working together in parallel configuration, and the tests show that each TES is working fine.

4.3 Data analysis by the PCA method.

As known [see Ref. 14 and refs therein] semiconductors absorbers are expected to develop at sub-K temperatures also an out-of-equilibrium phonon family, so called Athermal that is developed before the usual thermal component (the thermal component rises when the athermal decays): the pulse is a combination of both the components (see Fig. 9).

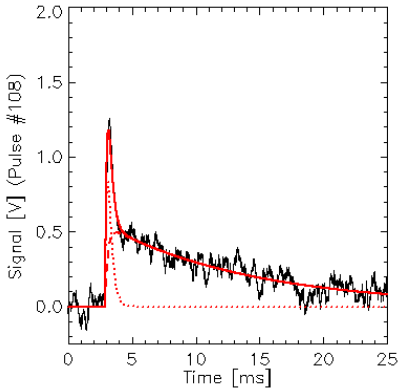

Figure 9. Results of the double pulse fitting procedure over the triggered pulses (solid red line). Dotted red line and dashed red line respectively represent the athermal and the thermal component of the pulses (Color figure online).

The Athermal, being quite fast, is expected to be used as flag to apply the veto to the particle bkg. Routinely, to better understand the detector physics, we try to disentangle the athermals from the thermals to get amplitudes, timing, etc… Since the athermals are the triggers to open the veto window, but their content energy is few percent with respect to the total deposited energy whose major part is connected to the thermals, it's important to study the detector threshold being this parameter important to reach high particle rejection efficiency (the wider the detector energy bandwidth, the higher the particle flux the CryoAC is able to veto). As reported in Table 1, the requirement is 20 keV.

We usually adopt two methods in order to study the pulses: the raw analysis of the acquired data, and the "double-pulse" fitting procedure in order to have more precise information (see Fig. 9).

Here we show the results of the PCA (Principal Component Analysis) method we have for the first time applied (see Ref. 15 for details). It is a quite interesting technique to be applied to noisy data, so important to have an optimum evaluation of the energy spectra, so the threshold. The data used for are related to the AC-S7 sample (see Ref. 12 for details, and Refs. Therein).

The Principal Component Analysis is a statistical procedure that allows to represent a complex dataset in terms of a small set of orthogonal components that have the largest variance (Principal Components). The goal is to represent each pulse as the linear combination of the Principal Components of the signal, which are selected from the eigenvectors of the time covariance matrix of the pulses. In this way it is possible to identify the significant characteristic pulse shape components, filtering out the noise, as model-independent analysis. The Principal Components can be then combined to form a representation of the pulses energy, obtaining the energy spectra.

The sample has been illuminated by a ^{241}Am shielded radioactive source, so we mainly expect the ~ 60 keV line.

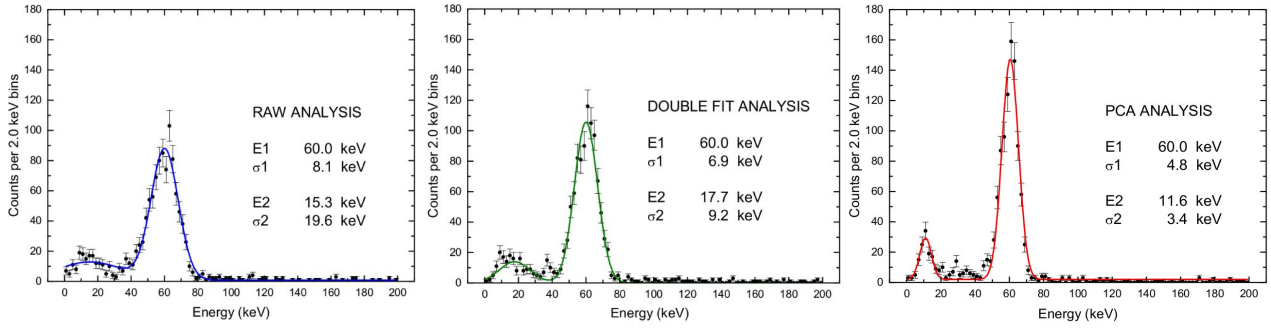

Figure 10. From Left to Right: energy spectra from the raw, the double pulse, and the PCA techniques (Color figure online).

The analysis result is shown in Fig. 10. It is shown that PCA provides a more narrow 60 keV line, and a threshold of about 20 keV. The bump around 10 keV is compatible with the expected Compton edge from 60 keV photo-peak (11.4 keV) whose shape is due to the convolution with the instrumental response.

5. STRUCTURAL ISSUES: ASPECTS ABOUT MODAL ANALYSIS, AND VIBRATIONS

Mechanical analysis is on-going to face structural issues due to the CryoAC geometry[16]. Here we report some preliminary results about modal analysis (Fig. 11) and the directional deformation along the vertical direction (Fig. 12).

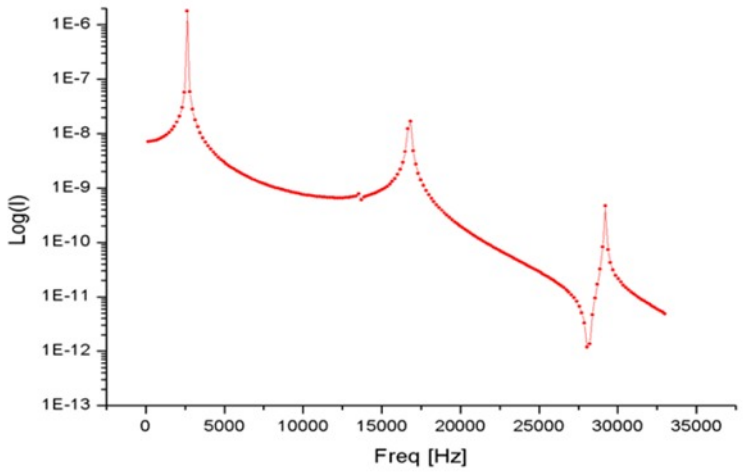

Figure 11. CryoAC 4 pixels array: modal analysis (Color figure online).

The modal analysis provides the following first eigenfrequencies: ~2.7 kHz, ~17 kHz, ~30 kHz. The first resonance frequency results to be sufficiently high with respect to the mechanical environment expected for the launch.

The Fig. 12 shows an interesting result about the vibration analysis which is quite important being the top surface of the CryoAC (i.e., the absorber) at about 500 μm distance from the Silicon wafer-substrate of the TES-array. To perform this simulation has been applied a random vibration spectra (Fig. 12 - Left). The simulation shows that the expected maximum deflection is about 2 μm meaning that, though it is a quite preliminary simulation, there is room to optimize the design.

Both the previous results have to be consolidated, but they show at present not particular showstopper in continuing along the 4-pixels separated CryoAC design.

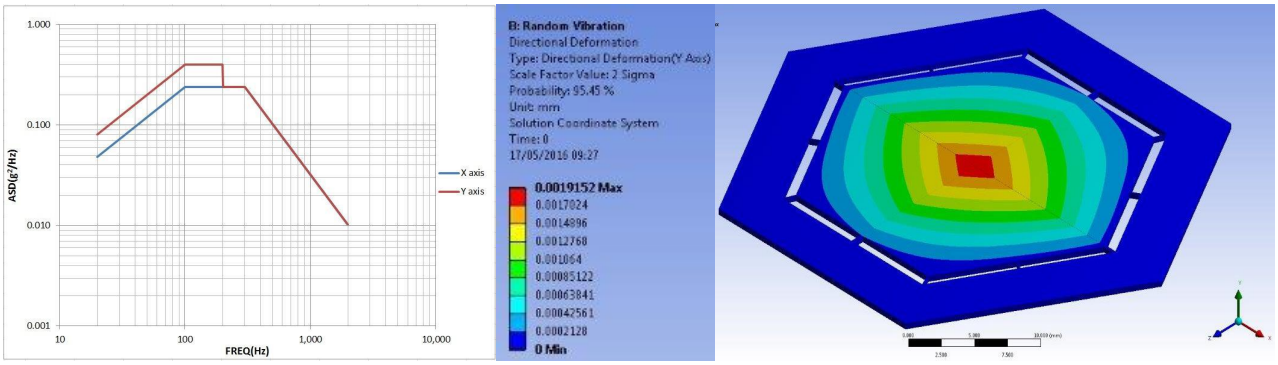

Figure 12. Left - FPA random vibration spectra (credits CNES/SRON). Right - Directional deformation along the vertical direction (y axis) (Color figure online).

6. PROGRAMMATIC ASPECTS: SOME INFO ABOUT THE NEXT ACTIVITIES

Here we provide a very brief overview of the CryoAC Phase A program. The following Fig. 13 shows the ATHENA master plan inside which the CryoAC activities have to be inserted: the reference is the FPA route. The conclusion of the Phase A is expected at the end of 2017.

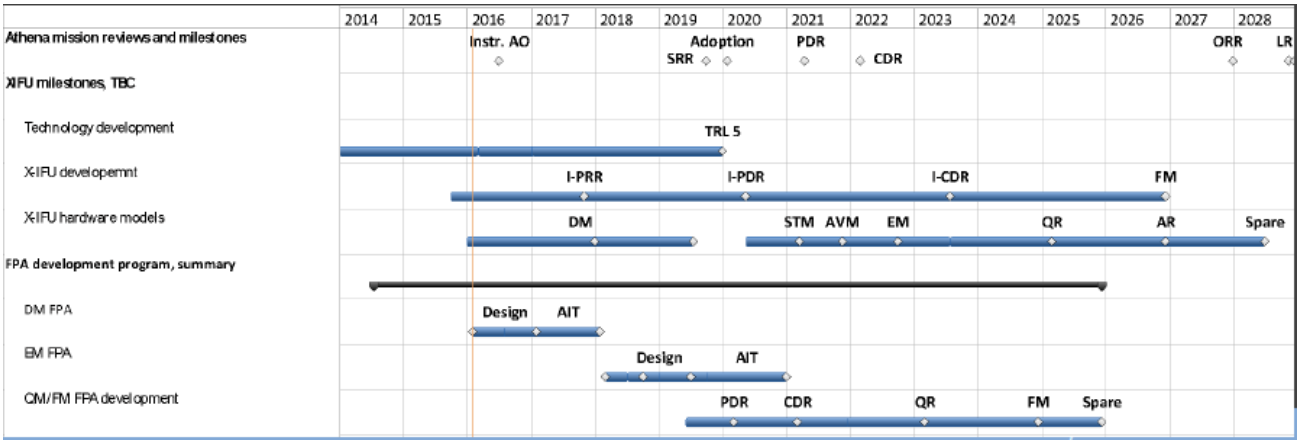

Figure 13. ATHENA/X-IFU/FPA master plan (Credits CNES/SRON) (Color figure online).

The CryoAC activities we have to face in the context of the Phase A route are:

1. TRL-5 demonstration before the adoption
2. Other nominal phase A activities

About the first point the program will be realized by:

- DM1 (single pixel): functional and reduced performance testing (CryoAC detector)
- DM2 (STM of the CryoAC full array)
  - Completion of the TRL-5 demonstration with mechanical vibrations

The DM2 will be implemented with a representative manufacturing mask. It will be not simply a structural model but it is a first model towards the development of the EM having on board also a deposited TES network. It is expected by Q1 2017 the delivery to SRON of the DM1 for integration and test inside their cold head, and on Q3 2017 the DM2.

The other Phase A activities to be pursued are:

- Standard phase A activities:
  - Preliminary Requirement specs
  - Preliminary performance budget
  - Trade-off studies
  - Conceptual design
  - Mass/power/data rate/etc budget
  - I-PRR data package preparation
- Other activities:
  - CryoAC + CFEE preliminary design and breadboarding (hexagonal array with 1-2 active pixels, TBC) towards the EM FPA

There is also a parallel path related to the bkg study. They have a direct impact not only on the CryoAC design, but also on the FPA design and the magnetic diverter[9]. As reported above most of the work is framed in the context of the AREMBES activities. The main tasks to be addressed are:

- Definition of the Geant4 Physics settings:
  - Proton reflection on the optics
  - E.M. physics (electron back scattering, etc.)
- Consolidation of the requirements for the magnetic diverter
- Feedbacks from the AREMBES program:
  - L2 particle environment
  - Mass model final definition
- Improvement of the confidence level on the Geant4 simulation results
- Update of the bkg estimation

7. CONCLUSIONS

A brief overview of the CryoAC activities has been discussed.
It involves bkg assessment having impact also on the FPA design (i.e., in turn the X-IFU science), detector requirements and specifications, electronics from the cold to the warm side, prototype characterization, structural analysis and programmatic aspects. All the activities are in good shape on a robust path to follow. From the technological point of view the next step is the development and test of the single pixel DM by Q1 2017.
More details about the sections shown so far can be found in the accompanying papers [Refs. 9, 13, 15 ,16].

ACKNOWLEDGEMENT

This work has been supported by ASI (Italian Space Agency) through the Contract n. 2015-046-R.0. The authors acknowledge also CNES, IRAP and SRON for the provided material.

REFERENCES

[1] Nandra, K., Barret, D., Barcons, X., Fabian, A., den Herder, J.-W., Piro, L., Watson, M., Adami, C., Aird, J., Afonso, J. M., and et al., "The Hot and Energetic Universe: A White Paper presenting the science theme motivating the Athena+ mission," 2013arXiv1306.2307N (2013).

[2] Barret, D., den Herder, Jan-Willem, Piro, L., T. L. Trong, X. Barcons, "The ATHENA X-ray Integral Field Unit", in this proceeding, paper 9905-83 (2016).

[3] Rau, A., Meidinger, N., Nandra, K., et al, "The Hot and Energetic Universe: The Wide Field Imager (WFI) for Athena+", 2013arXiv1308.6785, (2013).

[4] Lotti, S., Perinati, E., Natalucci, L., Piro, L., Mineo, T., Colasanti, L., Macculi, C., Federici, M., Martino, B., "An efficient method for reducing the background of microcalorimeters applied to ATHENA-XMS", Proc. of SPIE, Vol. 8443 84435H-1, (2012).

[5] SREM monitor, http://space-env.esa.int/index.php/ESA-ESTEC-Space-Environment-TEC-EES/articles/first-srem-data-from-herschelplanck.html

[6] Geotail, http://science.nasa.gov/missions/geotail/

[7] Wind, http://wind.nasa.gov/

[8] W. C. Blackwell et al., "Charged Particle Environment for NGST: Model Development", Proc. of SPIE Vol. 4013, 908 (2000).

[9] Lotti, S. et al., "Updates on the background estimates for the X-IFU instrument onboard of the ATHENA mission", in this issue, paper 9905-191 (2016).

[10] Thien Lam Trong et al., "X-IFU Instrument: technical challenges and preliminary design" in this issue, paper 9905-84 (2016).

[11] Macculi, C. et al., "The Cryogenic AntiCoincidence detector for ATHENA: the progress towards the final pixel design", Proc. of SPIE Vol. 9144, 91445S, (2014).

[12] Macculi, C. et al., "The Cryogenic AntiCoincidence detector for the ATHENA X-IFU: design aspects by Geant4 simulation, and preliminary characterization of the new single pixel", J Low Temp Phys DOI 10.1007/s10909-015-1439-y, (2016).

[13] Biasotti, M. et al., "The new cryogenic silicon monolithic micro-bridged AntiCoincidence detector for the XIFU of ATHENA,", in this issue, paper 9905-187 (2016).

[14] Macculi, C. et al., "The Cryogenic AntiCoincidence Detector Project for ATHENA+: An Overview Up to the Present Status", J Low Temp Phys, 176, (2014).

[15] D'Andrea, M. et al., "The Cryogenic Anti-Coincidence detector for ATHENA X-IFU: pulse analysis of the AC-S7 single pixel prototype", in this issue, paper 9905-185 (2016).

[16] Corsini, D. et al., "The mechanical and EM simulations of the CryoAC for the ATHENA X-IFU",in this issue, paper 9905-186 (2016).